Hydrothermal synthesis, phase evolution, and optical properties of Eu^{3+}-doped $KF–YF_3$ system materials

Chunyan Cao
College of Mathematics and Physics, Jinggangshan University, Ji'an 343009, China

Hyun Kyoung Yang, Byung Kee Moon, Byung Chun Choi, and Jung Hyun Jeong[a)]
Department of Physics, Pukyong National University, Busan 608-737, Korea

Kwang Ho Kim
School of Materials Science and Engineering, Pusan National University, Busan 609-735, Korea

(Received 28 June 2012; accepted 30 August 2012)

Through a polyethylene-glycol-assisted hydrothermal method, a series of potassium fluoride (KF)–Yttrium (III) fluoride (YF_3) system materials have been synthesized. By controlling the reactant ratios of KF: rare earth ions (RE^{3+}), the hydrothermal temperatures, and the pH values of the prepared solutions, the final products can evolve among the orthorhombic phase of YF_3 and/or the tetragonal phase of potassium triyttrium decafluoride (KY_3F_{10}) and/or the cubic phase of potassium yttrium tetrafluoride (KYF_4). The final products are characterized by the x-ray diffraction (XRD) patterns, the field-emission scanning electron microscopy (FE-SEM) images, the energy-dispersive spectroscopy (EDS) patterns, the photoluminescence (PL) spectra, and the luminescent dynamic decay curves. The XRD patterns of the samples suggest the phase evolution of the final products. The FE-SEM images and the EDS patterns prove that. Europium ion (Eu^{3+}) acting as a probe, its PL spectra and the luminescent decay curves all put together prove the phase evolution of the final products. The research can be extended to study the other $KF–REF_3$ system materials.

I. INTRODUCTION

Over the past decades, rare earth compounds have been extensively studied because of their practical and potential applications in high-performance magnets, luminescent devices, catalysts, photovoltaics, biological labels, and other functional materials based on the electronic, optical, and chemical characteristics arising from 4*f* electrons.[1–5] Among them, the rare-earth-doped fluorides based on $AREF_4$ (A = alkali metal, RE = rare earth) have been investigated for several decades due to their unique luminescent, ferromagnetic, insulating/magnetic, and piezoelectric properties and wide applications in laser devices, three-dimensional flat-panel displays, and low-intensity infrared imaging.[6–10] Fluoride host materials provide some distinct advantages owing to the low frequency phonons usually observed in their crystal lattices.[11,12] Usually, rare earth ions (RE^{3+}) doped into fluoride hosts display low probabilities for multiphonon relaxation processes, resulting in long lifetimes of their excited states and high luminescence quantum yields. For example, the hexagonal phase of sodium yttrium fluoride ($NaYF_4$) is considered as the most efficient host material for green and blue upconversion phosphors until now.[13] Lithium gadolinium tetrafluoride ($LiGdF_4$) is an outstanding host for down-conversion luminescence, for which the quantum efficiency is close to 200%.[14] Rare-earth-doped single crystals of KYF_4 are excellent solid-state laser materials, and laser action has been observed for ytterbium ions (Yb^{3+}), thulium ions (Tm^{3+}), and holmium ions (Ho^{3+}) in the KYF_4 lattice.[15,16] Recently, due to both their structural and optical properties, the RE^{3+}-doped $KF–REF_3$ (RE = Y, Gd) system materials have received more and more attention.[17–23] In the present article, we will research the synthesis, phase evolution, and optical properties of europium ion (Eu^{3+})-doped $KF–YF_3$ system materials.

In recent years, materials scientists have explored various synthetic strategies for the syntheses of reproducible and controllable nanocrystals with uniform size, morphology, and chemical composition. Dramatic efforts have been dedicated to synthesize rare earth fluoride nano-/microcrystals with uniform size and shape. In particular, high quality, such as monodisperse, single-crystalline, well-shaped, and phase-pure fluoride nanocrystals have been fabricated successfully due to their potential applications in biology and medicine. There are several successful methodologies for preparation of fluorides that have been well reviewed by Lin.[4] The hydrothermal treatment as a typical solution approach has been proved to be effective and convenient in preparing various inorganic materials with diverse controllable morphologies and architectures.[24] Especially, the hydrothermal method is relatively simple, and easy for

[a)]Address all correspondence to this author.
e-mail: jhjeong@pknu.ac.kr
DOI: 10.1557/jmr.2012.331

 © Materials Research Society 2012

https://doi.org/10.1557/jmr.2012.331 Published online by Cambridge University Press

implementation as also for production of a large amount of products. Therefore, the hydrothermal route has been adopted for the synthesis of $KF–YF_3$ system materials in the study reported in the present article.

As the most frequently used activator ion in luminescent materials, the Eu^{3+} mainly shows emissions in the red range due to transitions of $^5D_0 \rightarrow {}^7F_J$ ($J = 1, 2, 3, 4$). It is well known that the Eu^{3+} is a good probe for the chemical environment of the lanthanide ion. The $^5D_0 \rightarrow {}^7F_1$ and $^5D_0 \rightarrow {}^7F_2$ are typical magnetic dipole and electric dipole transitions, respectively, and the relative intensities of the two emissions depend strongly on the local symmetry of the Eu^{3+}. In a site with inversion symmetry the magnetic dipole transition $^5D_0 \rightarrow {}^7F_1$ is dominating, and in a site without inversion symmetry the electric dipole transition $^5D_0 \rightarrow {}^7F_2$ is stronger. In the present study, by controlling the reactant ratios ($KF:RE^{3+}$), the hydrothermal temperatures, and the pH values of the prepared solutions, the Yttrium (III) fluoride (YF_3), potassium yttrium tetrafluoride (KYF_4), and potassium triyttrium decafluoride (KY_3F_{10}) materials have been synthesized through a polyethylene glycol (PEG)-assisted hydrothermal method. Due to its sensitivity to local symmetry, the Eu^{3+} exhibits different optical properties and luminescence dynamics in the final products.

II. EXPERIMENTAL PROCEDURE

The samples were synthesized through a PEG-assisted hydrothermal method. The raw materials yttrium oxide (Y_2O_3) (99.99%, Sigma-Aldrich, Shanghai, China), europium (III) oxide (Eu_2O_3) (99.99%, Sigma-Aldrich, Shanghai, China), potassium fluoride (KF) (99+%, Sigma-Aldrich, Germany), and PEG (M_n = 8000, Sigma-Aldrich, Toyko, Japan) were all purchased from Aldrich and used directly without further purification. The PEG stock solution (5 wt%) was prepared by dissolving PEG in deionized water. The rare-earth trichloride ($RECl_3$) stock solution [RE = yttrium (Y), europium (Eu), Y:Eu = 9:1, 0.5 M] was prepared by dissolving the stoichiometrical Y_2O_3 and Eu_2O_3 in hydrochloric acid at elevated temperatures. In a typical synthesis procedure, 4 mL of $RECl_3$ solution was added into 21 mL of PEG solution. The obtained solution was stirred for 20 min, and then a 25 mL of PEG solution containing 16 mmol of KF was dropwise added. After agitation for another 15 min, the as-obtained milky solution was transferred into 70 mL of Teflon bottle held in a stainless steel autoclave, sealed, and maintained at 180 °C for 12 h. As the autoclave cooled down to room temperature in natural air under ambient conditions, the precipitates were separated by centrifugation, washed with ethanol and deionized water, and then dried in air at 60 °C for 24 h. Other conditions, such as the reactant ratios of $KF:RE^{3+}$, the hydrothermal temperatures, and the pH values of prepared solutions, have been adopted to study the effects of the above factors on the crystalline phases and optical properties of the final products. For convenience, the final products synthesized at 180 °C with $KF:RE^{3+}$ equaling 3, 3.5, 4, 6, 8, 12, 16, and 24 are denoted as Y3K, Y3.5K, Y4K, Y6K, Y8K, Y12K, Y16K, and Y24K, respectively. The final products synthesized with $KF:RE^{3+}$ = 8 at 60, 100, 140, 180, 220, and 260 °C are denoted as Y60, Y100, Y140, Y180 (Y8K), Y220, and Y260, respectively. And the final products synthesized at 180 °C ($KF:RE^{3+}$ = 8) with pH values equaling 1, 5.5, and 10 are named as YpH1, YpH5.5 (Y8K), and YpH10, respectively. All the samples are treated hydrothermally for 12 h.

The crystalline structures of the obtained samples were characterized by x-ray diffraction (XRD; Xpert/MPD, Eindhoven, Netherlands) with Cu K_α (λ = 1.5406 Å) radiation. The morphology and size of the obtained samples as well as the energy-dispersive spectroscopy (EDS) were observed with field-emission scanning electron microscopy (FE-SEM, JSM-6700F, JEOL, Tokyo, Japan). The room-temperature photoluminescence (PL) excitation and emission spectra were recorded using a Photon Technology International (PTI, Birmingham, NJ) fluorimeter with a Xe-arc lamp of power 60 W as excitation source. The luminescent dynamic decay curves of Eu^{3+} $^5D_0 \rightarrow {}^7F_1$ transition were measured using a phosphorimeter attachment to the PTI with a Xe-flash lamp (25 W) as excitation source.

III. RESULTS AND DISCUSSION

A. Crystalline phase

Figure 1 shows XRD patterns of the final products synthesized at 180 °C with different reactant ratios of $KF:RE^{3+}$. The amount of KF has considerable impact on the crystalline phase of final products. As shown in Fig. 1(a), the XRD pattern of the sample Y3K can be well indexed to the orthorhombic phase of YF_3 [Joint Committee on Powder Diffraction Standards (JCPDS) 74-0911], indicating that the potassium ion (K^+) does not participate in the chemical reaction. When the ratio of KF to RE^{3+} increases to 3.5, new peaks marked as * emerge in the XRD pattern of the sample Y3.5K. The new peaks can be indexed to the tetragonal phase of KY_3F_{10} (JCPDS 27-0465), suggesting that the sample Y3.5 is a mixture of the orthorhombic phase of YF_3 and the tetragonal phase of KY_3F_{10}. The pure tetragonal phase of KY_3F_{10} is obtained with the ratio of KF to RE^{3+} increasing to 4, as presented in Figs. 1(a) and 1(b). The sample Y6K remains the tetragonal phase of KY_3F_{10}, as shown in Fig. 1(b). Some diffraction peaks disappear in sample Y8K. The diffraction peaks can be indexed to the cubic phase of $NaYF_4$ (JCPDS 06-0342, a = 5.45 Å), but the positions of the diffraction peaks move to lower angle for larger ionic radius of K^+ replacing Na^+, which means that the sample Y8K is isostructural to that of the cubic phase of $NaYF_4$. Based on the assumption of the isostructure, a cubic unit cell with a = 5.65 Å was obtained by using the MDI

https://doi.org/10.1557/jmr.2012.331 Published online by Cambridge University Press

JADE 5.0 software. The calculated diffraction peaks (red solid dot) are also plotted underside of the experimental pattern of sample Y8K. Increasing the ratio of KF to RE^{3+}, the samples Y12K, Y16K, and Y24K remain as the cubic phase, as shown in Fig. 1(b). The XRD data suggest that the amount of KF has considerable impact on the crystalline phases of the final products. With the increase of the amount of KF, the final products evolve from the orthorhombic phase of YF_3 to the tetragonal phase of KY_3F_{10} to the cubic phase of KYF_4 finally. Next, the KF:RE^{3+} = 8 condition was selected to investigate the effects of the hydrothermal temperatures and the pH values of the prepared solutions on the final products.

Figure 2 presents the XRD patterns of the final products synthesized at different hydrothermal temperatures with KF:RE^{3+} = 8 and pH = 5.5. The samples synthesized under lower temperatures (60, 100, 140, and 180 °C) tend to be the cubic phase of KYF_4 and the reference data cubic phase of $NaYF_4$ (JCPDS 06-0342) are also listed in Fig. 2. Increasing the hydrothermal temperature further, new peaks emerge in the samples Y220 and Y260. The two samples can be indexed to the tetragonal phase of KY_3F_{10} (JCPDS 27-0465). The hydrothermal temperature dependent XRD patterns of the samples suggest that the lower hydrothermal temperature is beneficial for the formation of the cubic phase of KYF_4 and the higher hydrothermal temperature is good for the formation of the tetragonal phase of KY_3F_{10}.

Figure 3 illustrates the XRD patterns of the samples synthesized at 180 °C (KF:RE^{3+} = 8) with different pH values of prepared solutions. The sample YpH1 synthesized with pH value equaling 1 can be well indexed to the tetragonal phase of KY_3F_{10} (JCPDS 27-0465). From the narrowed peaks of the diffractions peaks, we can infer that the particle size of the sample YpH1 is relatively larger than that of the other KY_3F_{10} samples. The samples YpH5.5 (Y8K) and YpH10 synthesized with pH value equaling 5.5 and 10 can both be indexed to the cubic phase of KYF_4. For clarity, the reference data of the cubic phase of $NaYF_4$ (JCPDS 06-0342) and the tetragonal phase of KY_3F_{10} (JCPDS 27-0465) are also listed in the figure. The

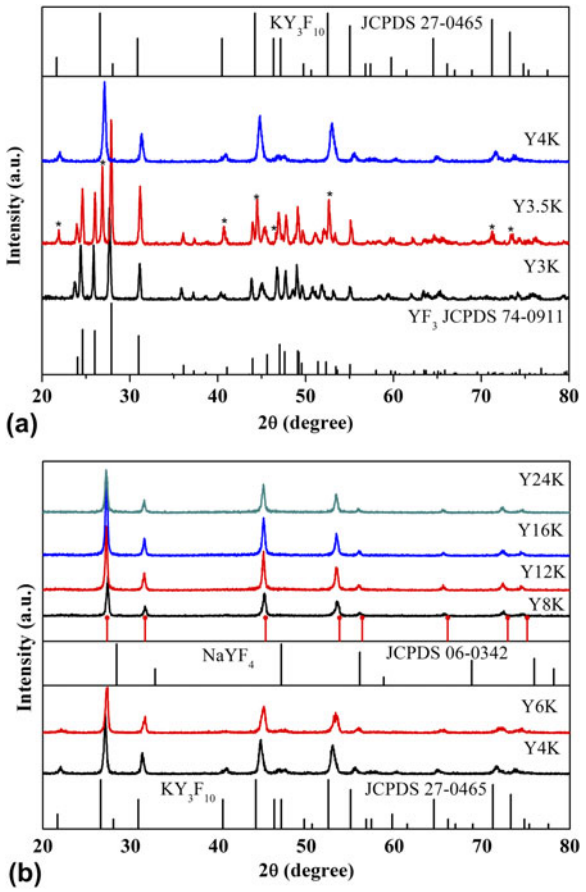


FIG. 1. XRD patterns of samples synthesized at 180 °C with different reactant ratios of KF:RE^{3+} and corresponding standard data.

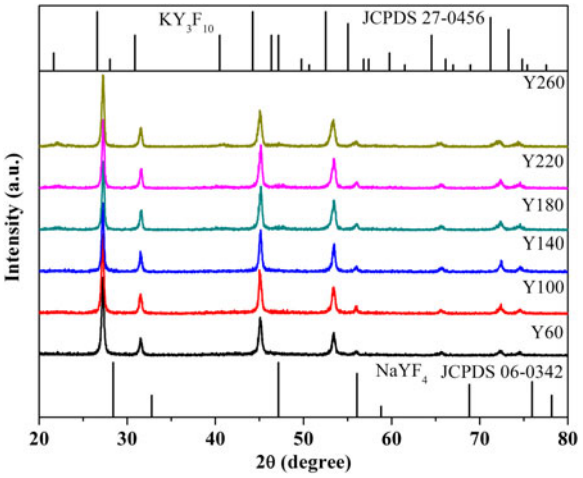


FIG. 2. Hydrothermal temperature dependent XRD patterns of final products with KF:RE^{3+} = 8:1.

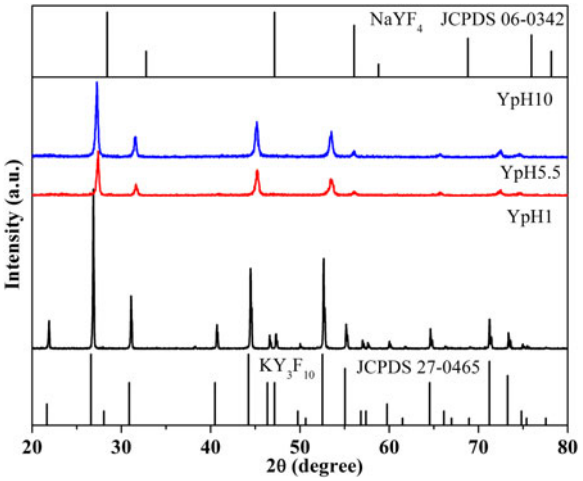


FIG. 3. XRD patterns of samples synthesized at 180 °C (KF:RE^{3+} = 8) with different pH values of prepared solutions.

https://doi.org/10.1557/jmr.2012.331 Published online by Cambridge University Press

XRD data suggest that the strong acidic environment is propitious for the formation of the tetragonal phase of KY_3F_{10} and the weak acidic environment and the alkaline environment are favorable for the cubic phase of KYF_4.

B. Morphology

In addition to the crystalline phases of the samples, the morphology and the constituents of some representative samples have also been investigated. Figure 4(a) shows an FE-SEM image of the sample Y3K (YF_3). The YF_3 is octahedron-shaped with an edge length of 2–4 μm. The EDS pattern of the sample Y3K in Fig. 4(b) confirms that the constituents of the sample are composed of fluorine (F), yttrium (Y), and europium (Eu), indicating that the K^+ does not participate in the chemical reaction. In addition to the octahedron-shaped particles, some nanoparticles emerge in the sample Y3.5K as shown in Fig. 4(c). The sample Y4K [Fig. 4(d)] is made up of some particles with an average size of 100 nm. The evolution of the FE-SEM images conforms well to the XRD data, which suggests that the concentration of KF also has considerable impact on the morphology of the samples.

The FE-SEM image of Y8K, which is the cubic phase of KYF_4, is shown in Fig. 5(a), and the corresponding EDS pattern is shown in Fig. 5(b). The sample Y8K is composed of spherical particles with an average size of 70 nm. The EDS pattern of the sample suggests that the Y8K is composed of potassium (K), Y, F, and Eu. The FE-SEM image and the EDS pattern of the sample YpH1 are shown in Figs. 5(c) and 5(d), respectively. The sample YpH1 is the tetragonal phase of KY_3F_{10}. As shown in Fig. 5(c), the sample KY_3F_{10} is composed of polyhedral morphology particles with an average size of 5–8 μm. The sample Y4K [Fig. 4(d)] is also the tetragonal phase of KY_3F_{10}, but the size and the morphology have great differences with those of YpH1. The EDS pattern of the sample in Fig. 5(d) suggests that the YpH1 is also composed of K, Y, F, and Eu. The EDS patterns of the samples Y8K and YpH1 indicate that the two samples are both composed of K, Y, F, and Eu, but the relative proportions of the compositions are different, which also suggests that the crystalline phases of the two samples are different.

The morphologies of some other representative samples are also studied. The FE-SEM images of YpH10, Y24K, Y100, and Y260 are presented in Figs. 6(a)–6(d), respectively. The sample YpH10 is the cubic phase of KYF_4, which is made up of sphere-like particles with an average size of 60 nm. The sample Y24K is also the cubic phase of KYF_4, which has smaller size than that of Y8K [Fig. 5(a)] or YpH10 [Fig. 6(a)]. The sample Y100 is the cubic phase of KYF_4, which is also composed of spherical particle. With the hydrothermal temperature increasing to 260 °C, the average particle size of the sample Y260 becomes larger. As discussed earlier, the crystalline phase of the samples evolved from the cubic phase of KYF_4 to the tetragonal phase of KY_3F_{10} with the hydrothermal temperature increasing. The morphology of the sample Y260 is similar to that of Y4K as shown in Fig. 4(d).

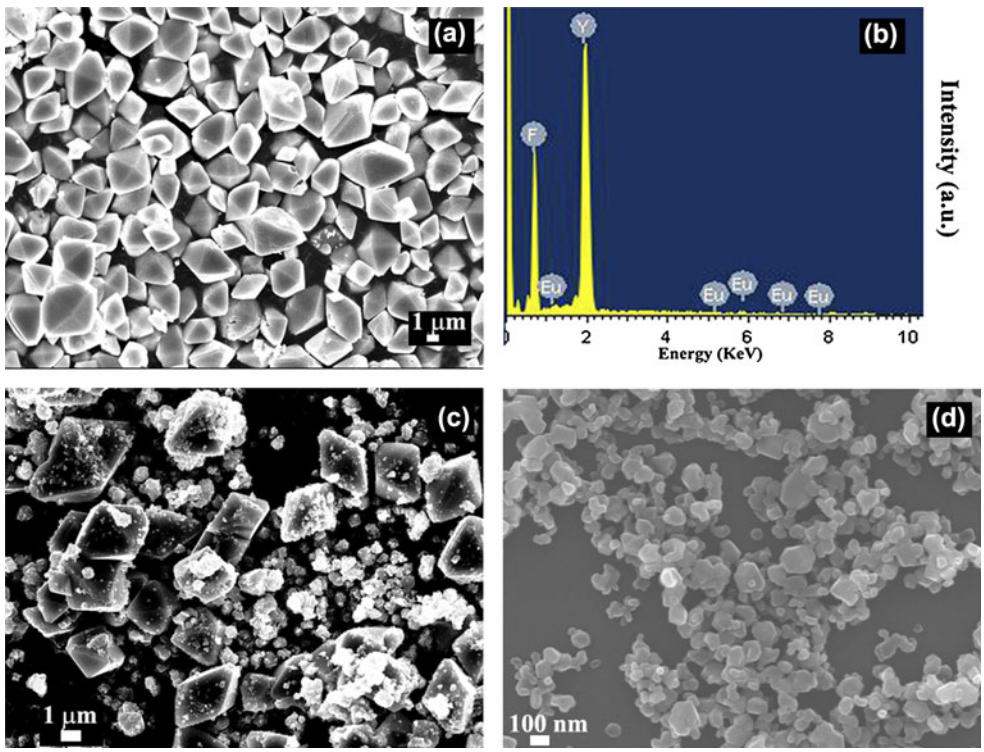


FIG. 4. FE-SEM images of (a) Y3K, (c) Y3.5K, and (d) Y4K. (b) EDS pattern of Y3K.

https://doi.org/10.1557/jmr.2012.331 Published online by Cambridge University Press

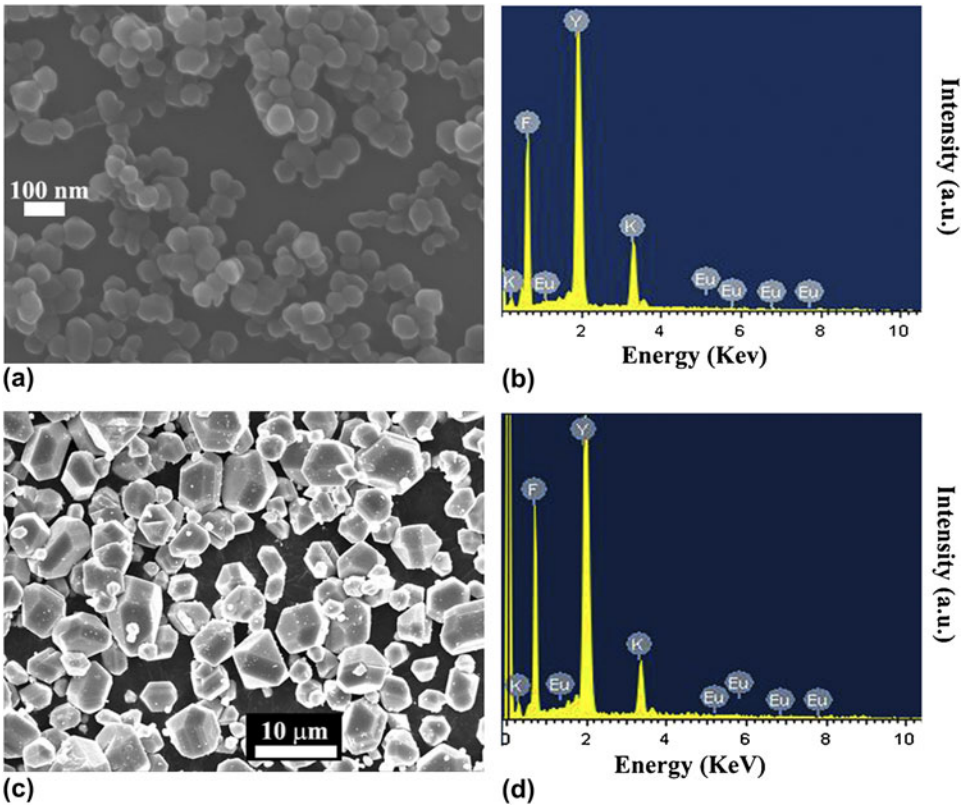


FIG. 5. FE-SEM image (a) and EDS pattern (b) of Y8K, FE-SEM image (c) and EDS pattern (d) of YpH1.

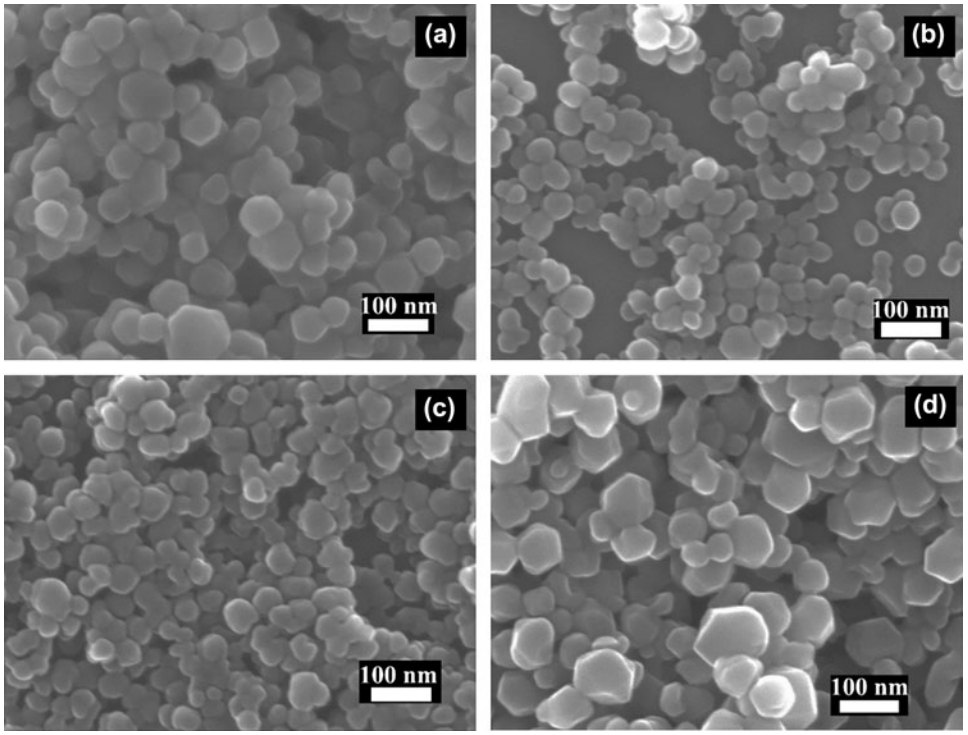
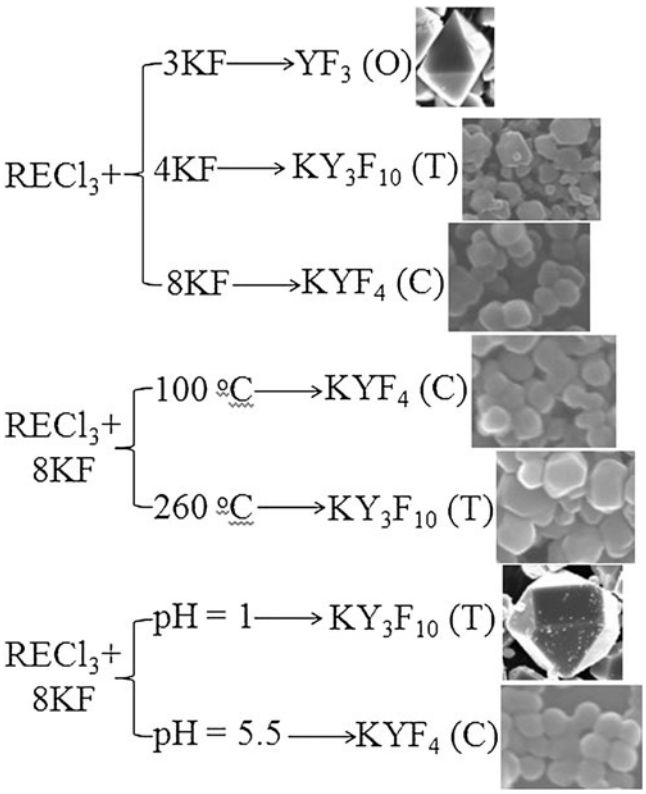


FIG. 6. FE-SEM images of (a) YpH10 (b) Y24K (c) Y100 (d) Y260.

https://doi.org/10.1557/jmr.2012.331 Published online by Cambridge University Press

In brief, the formation, the crystalline phase, and the morphology evolution of the samples are summarized in Scheme 1. Based on the analysis of the above crystalline phases and morphologies of the $KF–YF_3$ system materials, a possible formation and phase evolution process of the samples is proposed. For the samples synthesized with different reactant ratios of $KF:RE^{3+}$, it is easy to understand the phase evolution of the final products. When $KF:RE^{3+} = 3:1$, the amount of F^- is just adequate for the formation of the orthorhombic phase of REF_3 and the K^+ cannot participate in the chemical reaction. When the ratio of $KF:RE^{3+} = 3.5:1$, the amount of F^- is surplus to form the orthorhombic phase of REF_3 and the K^+ can partially participate in the chemical reaction to form the tetragonal phase of KY_3F_{10}. With the increase of the ratio of $KF:RE^{3+}$ further, the amount of F^- is enough to form the tetragonal phase of KY_3F_{10} then to the cubic phase of KYF_4. For the sample synthesized with different hydrothermal temperatures and different pH values of the prepared solutions, the results suggest that a higher synthesis temperature and a lower pH value of the prepared solution are good for the formation of the tetragonal phase of KY_3F_{10}. Likewise, a lower synthesis temperature and a higher pH value of the prepared solution are beneficial for the formation of the cubic phase of KYF_4. The phase evolution of the $KF–YF_3$ system materials is relatively complex and the formation mechanism needs more exploration. The related work as investigated so far is insufficient to be conclusive.



SCHEME 1. Formation, crystalline phase, and morphology evolution of final products. O represents orthorhombic phase, T represents tetragonal phase, and C represents cubic phase.

C. Optical properties

Figure 7 shows some representative PL excitation and emission spectra of the 1 mol% Eu^{3+}-doped Y3K (YF_3), Y4K (KY_3F_{10}), and Y8K (KYF_4). In the three samples, the excitation spectra (the black line in the left part of the figure) are similar which are all consistent with respect to the characteristic excitation lines of Eu^{3+} within its $4f^6$ configuration from 230 to 500 nm. For example, in sample Y8K (KYF_4), the excitation peaks can be clearly assigned from the ground state $^7F_0$ to different excited states: $^5H_6$ (320 nm), $^5D_4$ (363 nm), $^5G_2$ (384 nm), and $^5L_6$ (395 nm) which is the strongest one, including those weak ones which have little contribution to the excitation of Eu^{3+}.[25] Excitation into the strongest $^7F_0 \rightarrow {}^5L_6$ transition of Eu^{3+} at 395 or 396 nm yields the emission spectra (the red line) of 1 mol% Eu^{3+}-doped Y3K (YF_3), Y4K (KY_3F_{10}), and Y8K (KYF_4) as shown in the right part of the figure, which consists of the emission lines of Eu^{3+} from the excited $^5D_{0,1,2}$ levels to the ^7F_J level. For example, in sample Y8K (KYF_4), there are emission peaks at 512 nm corresponding to the $^5D_2 \rightarrow {}^7F_3$ transition; 527, 535.5, and 554.5 (561) nm corresponding to the $^5D_1 \rightarrow {}^7F_0$, $^7F_1$, and $^7F_2$ transitions; and 590 and 594.5 nm for the $^5D_0 \rightarrow {}^7F_1$ transition, 614 and 622 nm for the $^5D_0 \rightarrow {}^7F_2$ transition, 652.5 nm for the $^5D_0 \rightarrow {}^7F_3$ transition, and 693.5 and 703.5 nm for the $^5D_0 \rightarrow {}^7F_4$ transition, respectively.[26,27] The emission spectra are dominated by the $^5D_0 \rightarrow {}^7F_1$, $^7F_2$ transitions. The $^5D_0 \rightarrow {}^7F_1$ transition is a magnetic dipole transition and not affected much by the crystal field around Eu^{3+} and the $^5D_0 \rightarrow {}^7F_2$ transition is an electric dipole transition and hypersensitive to the local environment. The asymmetric ratio (β) of the integrated intensity I($^5D_0 \rightarrow {}^7F_2$) (604–625 nm) to that of I($^5D_0 \rightarrow {}^7F_1$) (578–604 nm) can provide some

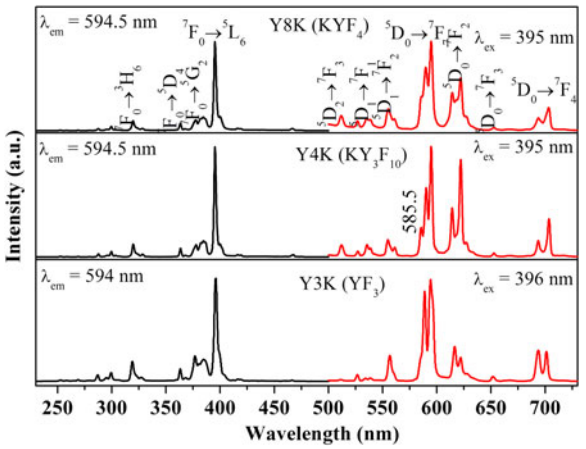


FIG. 7. PL excitation and emission spectra of samples Y3K (YF_3), Y4K (KY_3F_{10}), and Y8K (KYF_4).

https://doi.org/10.1557/jmr.2012.331 Published online by Cambridge University Press

TABLE I. Asymmetric ratio β values and lifetimes of $^5D_0 \rightarrow {}^7F_1$ transition [λ_{ex} = 395 nm, λ_{em} = 594.5 nm except Y3K (λ_{ex} = 396 nm, λ_{em} = 594 nm) and Y3.5K (λ_{ex} = 396 nm, λ_{em} = 594 nm)] of samples.

Sample	Composition	β	τ (ms)	Sample	Composition	β	τ (ms)
Y3K	YF_3	0.307	7.46 ± 0.04	Y60	KYF_4	0.674	12.23 ± 0.09
Y3.5K	$YF_3 + KY_3F_{10}$	0.370	7.99 ± 0.06	Y100	KYF_4	0.649	11.57 ± 0.08
Y4K	KY_3F_{10}	0.787	13.40 ± 0.09	Y140	KYF_4	0.624	10.34 ± 0.07
Y6K	KY_3F_{10}	0.715	13.45 ± 0.11	Y220	KY_3F_{10}	0.670	12.09 ± 0.09
Y8K	KYF_4	0.633	9.90 ± 0.07	Y260	KY_3F_{10}	0.682	9.88 ± 0.07
Y12K	KYF_4	0.642	11.28 ± 0.08	YpH1	KY_3F_{10}	0.724	7.37 ± 0.05
Y16K	KYF_4	0.643	12.52 ± 0.12	YpH10	KYF_4	0.676	12.76 ± 0.09
Y24K	KYF_4	0.630	10.61 ± 0.09	...	...	...	...

structural information such as distortion of ligand environment and site symmetry.[28] The β value of the sample Y8K (KYF_4) is about 0.633, indicating that the Eu^{3+} locates at a site without inversion symmetry in the host matrix. The PL emission spectrum of the sample Y4K (KY_3F_{10}) is some different from that of KYF_4. The splits of the transitions, such as $^5D_0 \rightarrow {}^7F_1$, $^5D_0 \rightarrow {}^7F_2$, $^5D_0 \rightarrow {}^7F_4$ are different. There is a distinct peak at 585.5 nm in the emission spectrum of the sample Y4K (KY_3F_{10}). And the β values of the asymmetric ratio in the sample Y4K (KY_3F_{10}) is 0.787, which are larger than that in the sample Y8K (KYF_4) meaning that the Eu^{3+} locates in a more asymmetric lattice site in KY_3F_{10} than that in KYF_4. The emission spectrum of YF_3 (Y3K) is also different from that of KY_3F_{10} or KYF_4. The β value in the sample YF_3 (Y3K) is only 0.307, suggesting that the Eu^{3+} locates in a most symmetric lattice site in the three samples. For clarity, the samples and the corresponding asymmetric ratio β values are listed in Table I. The β values of the different KYF_4 samples or the different KY_3F_{10} samples change slightly, which is partly caused by the crystalline size of the particles in the samples.

Figure 8 displays the representative luminescent dynamic decay curves monitoring at the $^5D_0 \rightarrow {}^7F_1$ transition of Eu^{3+} in samples Y3K (YF_3), Y4K (KY_3F_{10}), and Y8K (KYF_4). The decay curves can be well fitted by a single exponential function as $I(t) = I_0\exp(-t/\tau)$, where I_0 is the initial emission intensity at $t = 0$, τ is the 1/e lifetime of the $^5D_0$ level of Eu^{3+}. The lifetime in the YF_3 (Y3K) sample is 7.46 ± 0.04 ms, which is much shorter than that in the KY_3F_{10} (Y4K, τ = 13.40 ± 0.09 ms) sample or the KYF_4 (Y8K, τ = 9.90 ± 0.07 ms) sample. The deduced lifetimes of the $^5D_0$ level of Eu^{3+} are also listed in Table I. When Eu^{3+} locates in a more symmetric lattice site, the $^5D_0$ level of the Eu^{3+} has a shorter lifetime. On the contrary, the $^5D_0$ level of the Eu^{3+} has a longer lifetime when it locates in a more asymmetric lattice site. There is an exception that is the sample YpH1 (KY_3F_{10}). In the sample, the Eu^{3+} locates in a more asymmetric lattice site but the $^5D_0$ level of the Eu^{3+} has a shorter lifetime which is 7.37 ± 0.05 ms. As discussed in the foregoing, the KY_3F_{10} presents a larger size in the particles and crystallizes well, meaning low nonradiative rate, which finally results in a shorter lifetime of the D_0 level of the Eu^{3+} in the sample.

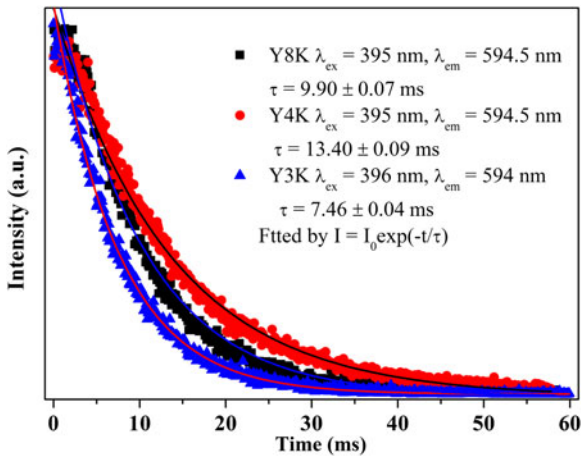


FIG. 8. Decay curves monitoring at $^5D_0 \rightarrow {}^7F_1$ transition of Eu^{3+} in samples Y3K (YF_3), Y4K (KY_3F_{10}), and Y8K (KYF_4).

IV. CONCLUSIONS

In conclusion, a series of $KF–YF_3$ system materials have been synthesized through a PEG-assisted hydrothermal method. With the increase of the reactant ratios of $KF:RE^{3+}$, the final products evolve from the orthorhombic phase of YF_3 to the tetragonal phase of KY_3F_{10} to the cubic phase of KYF_4 finally. With the increase of the hydrothermal temperatures, the final products evolve from the cubic phase of KYF_4 to the tetragonal phase of KY_3F_{10}. With the increase of the pH values of the prepared solutions, the final products inversely evolve from the tetragonal phase of KY_3F_{10} into the cubic phase of KYF_4. The XRD patterns, the FE-SEM images, and the EDS pattern of the samples suggest the phase evolution of the samples. The PL spectra and the luminescent decay curves of the doping Eu^{3+} also prove the phase evolution of the final products. The synthesis, the phase evolution, and the optical properties of Eu^{3+}-doped $KF–YF_3$ materials can be extended to study the other $KF–REF_3$ system materials.

https://doi.org/10.1557/jmr.2012.331 Published online by Cambridge University Press

ACKNOWLEDGMENTS

This research was supported by Basic Science Research Program through the National Research Foundation of Korea (NRF) funded by the Ministry of Education, Science and Technology (No. 2010-0022540) and also this research was supported by NCRC (National Core Research Center) program through the National Research Foundation of Korea funded by the Ministry of Education, Science and Technology (2010-0001–226). The first author thanks for the financial support of National Natural Science Foundation of China (Grant No. 61205217), the project of Young Excellent Doctor (JZB11001) of Jinggangshan University, and the project of the Key Subject of Atomic and Molecular Physics supported by Jiangxi Province (2011-1015), China.

REFERENCES

1. H.X. Mai, Y.W. Zhang, R. Si, Z.G. Yan, L.D. Sun, L.P. You, and C.H. Yan: High-quality sodium rare-earth fluoride nanocrystals: Controlled synthesis and optical properties. *J. Am. Chem. Soc.* **128**, 6426 (2006).
2. B. Yan and J.H. Wu: Facile composite synthesis and photoluminescence of NaGd(MoO4)2: Ln^{3+} (Ln = Eu, Tb) submicrometer phosphors. *J. Mater. Res.* **24**, 32 (2009).
3. M. Yu, H. Wang, C.K. Lin, G.Z. Li, and J. Lin: Sol–gel synthesis and photoluminescence properties of spherical SiO_2@$LaPO_4$:Ce^{3+}/Tb^{3+} particles with a core–shell structure. *Nanotechnology* **17**, 3245 (2006).
4. C.X. Li and J. Lin: Rare earth fluoride nano-/microcrystals: Synthesis, surface modification and application. *J. Mater. Chem.* **20**, 6831 (2010).
5. C-H. Liang, Y-C. Chang, Y-S. Chang, and S. Wu: Photoluminescence properties of Eu^{3+}-doped BaY_2ZnO_5 phosphors under near-ultraviolet irradiation. *J. Mater. Res.* **25**, 850 (2010).
6. N. Menyuk, K. Dwight, and J.W. Pierce: $NaYF_4$: Yb, Er—an efficient upconversion phosphor. *Appl. Phys. Lett.* **21**, 159 (1972).
7. J.L. Sommerdijk and A. Bril: Phosphors for the conversion of infrared radiation into visible light. *Philips Tech. Rev.* **34**, 1 (1974).
8. E. Downing, L. Hesselink, J. Ralston, and R. Macfarlane: A three-color, solid-state, three-dimensional display. *Science* **273**, 1185 (1996).
9. C.Y. Cao, H.K. Yang, J.W. Chung, B.K. Moon, B.C. Choi, J.H. Jeong, and K.H. Kim: Ce^{3+}/Tb^{3+} activated GdF_3, $KGdF_4$, and CeF_3 submicro/nanocrystals: Synthesis, phase evolution, and optical properties. *J. Mater. Res.* **26**, 2916 (2011).
10. S. Shionoya and W.M. Yen: *Phosphor Handbook* (CRC Press, Boca Raton, FL, 1999).
11. P.R. Diamente, M. Raudsepp, and F.C.J.M. van Veggel: Dispersible Tm^{3+}-doped nanoparticles that exhibit strong 1.47 μm photoluminescence. *Adv. Funct. Mater.* **17**, 363 (2007).
12. X.H. Liu, L.M. Wang, Z.Y. Wang, and Z.Q. Li: Synthesis of biocompatible and luminescent $NaGdF_4$:Yb, Er@Carbon nanoparticles in water-in-oil microemulsion. *J. Mater. Res.* **26**, 82 (2011).
13. K.W. Krämer, D. Biner, G. Frei, H.U. Güdel, M.P. Hehlen, and S.R. Lüthi: Hexagonal sodium yttrium fluoride-based green and blue emitting upconversion phosphors. *Chem. Mater.* **16**, 1244 (2004).
14. R. Wegh, H. Donker, K. Oskam, and A. Meijerink: Visible quantum cutting in $LiGdF_4$:Eu^{3+} through downconversion. *Science* **283**, 663 (1999).
15. P.E.A. Möbert, A. Diening, E. Heumann, G. Huber, and B.H.T. Chai: Room-temperature continuous-wave upconversion-pumped laser emission in Ho, Yb:KYF_4 at 756, 1070, and 1390 nm. *Laser Phys.* **8**, 210 (1998).
16. A. Braud, S. Girard, J.L. Doualan, M. Thuau, R. Moncorgé, and A.M. Tkachuk: Energy-transfer processes in Yb:Tm-doped KY_3F_{10}, $LiYF_4$, and BaY_2F_8 single crystals for laser operation at 1.5 and 2.3 μm. *Phys. Rev. B* **61**, 5280 (2000).
17. D.M. Yang, G.G. Li, X.J. Kang, Z.Y. Cheng, P.A. Ma, C. Peng, H.Z. Lian, C.X. Li, and J. Lin: Room temperature synthesis of hydrophilic Ln^{3+}-doped $KGdF_4$ (Ln = Ce, Eu, Tb, Dy) nanoparticles with controllable size: Energy transfer, size-dependent and color-tunable luminescence properties. *Nanoscale* **2**, 3450 (2012).
18. N. Kodama and Y. Watanabe: Visible quantum cutting through downconversion in Eu^{3+}-doped KGd_3F_{10} and KGd_2F_7 crystals. *Appl. Phys. Lett.* **84**, 4141 (2004).
19. T. Lee, L. Luo, W. Diau, T. Chen, B. Cheng, and C. Tung: Visible quantum cutting through downconversion in green-emitting K_2GdF_5:Tb^{3+} phosphors. *Appl. Phys. Lett.* **89**, 131121 (2006).
20. L.W. Yang, Y.Y. Zhang, J.J. Li, Y. Li, J.X. Zhong, and P.K. Chu: Magnetic and upconverted luminescent properties of multifunctional lanthanide-doped cubic $KGdF_4$ nanocrystals. *Nanoscale* **2**, 2805 (2010).
21. H-T. Wong, F. Vetrone, R. Naccache, H.L.W. Chan, J.H. Hao, and J.A. Capobianco: Water-dispersible ultrasmall multifunctional $KGdF_4$:Tm^{3+}, Yb^{3+} nanoparticles with near-infrared to near-infrared upconversion. *J. Mater. Chem.* **21**, 16589 (2011).
22. C.Y. Cao, H.K. Yang, J.W. Chung, B.K. Moon, B.C. Choi, J.H. Jeong, and K.H. Kim: Hydrothermal synthesis and enhanced photoluminescence of Tb^{3+} in Ce^{3+}/Tb^{3+}-doped $KGdF_4$ nanocrystals. *J. Mater. Chem.* **21**, 10342 (2011).
23. C.X. Li, Z.H. Xu, D.M. Yang, Z.Y. Cheng, Z.Y. Hou, P.A. Ma, H.Z. Lian, and J. Lin: Well-dispersed KRE_3F_{10} (RE = Sm–Lu, Y) nanocrystals: Solvothermal synthesis and luminescence properties. *CrystEngComm* **14**, 670 (2012).
24. J.H. Liang, Q. Peng, X. Wang, X. Zheng, R.J. Wang, X.P. Qiu, C.W. Nan, and Y.D. Li: Chromate nanorods/nanobelts: General synthesis, characterization, and properties. *Inorg. Chem.* **44**, 9405 (2005).
25. L.G. Deshazer and G.H. Dieke: Spectra and energy levels of Eu^{3+} in $LaCl_3$. *J. Chem. Phys.* **38**, 2190 (1963).
26. M. Yu, J. Lin, and J. Fang: Silica spheres coated with YVO_4:Eu^{3+} layers via sol−gel process: A simple method to obtain spherical core−shell phosphors. *Chem. Mater.* **17**, 1783 (2005).
27. F. Tao, Z.J. Wang, L.Z. Yao, W.L. Cai, and X.G. Li: Synthesis and photoluminescence properties of truncated octahedral Eu-doped YF_3 submicrocrystals or nanocrystals. *J. Phys. Chem. C* **111**, 3241 (2007).
28. X.Y. Chen and G.K. Liu: The standard and anomalous crystal-field spectra of Eu^{3+}. *J. Solid State Chem.* **178**, 419 (2005).

https://doi.org/10.1557/jmr.2012.331 Published online by Cambridge University Press